

AD-A033 898

AIR FORCE GEOPHYSICS LAB HANSCOM AFB MASS  
INTERPRETATION OF PPI VELOCITY DISPLAYS IN WIDESPREAD STORMS. (U)  
DEC 76 M J KRAUS, R J DONALDSON

F/G 4/2

UNCLASSIFIED

AFGL-TR-76-0283

NL

1 of 1  
AD-A033898



END

DATE  
FILMED  
2 - 77

11  
NWReprinted from Preprint Volume: 17th Conference on  
Radar Meteorology, Oct. 26-29, 1976, Seattle Wash.;  
Published by American Meteorological Soc., Boston, Ma.

222 1473

## INTERPRETATION OF PPI VELOCITY DISPLAYS IN WIDESPREAD STORMS

Michael J. Kraus and Ralph J. Donaldson, Jr.  
Air Force Geophysics Laboratory  
Hanscom AFB, Massachusetts 01731

## 1. INTRODUCTION

During the 1975-76 winter season AFGL's 5.4 cm wavelength Porcupine Doppler radar was used to observe New England's usual variety of stratiform-type storms. By using a Pulse Pair Processor (Novick, et al., 1975) and color displays (Jagodnik, et al., 1975) we were able to view each storm in real time with up to 1024 adjacent 1  $\mu$ s range gates. Once we were able to overcome our awe of the beautiful PPI patterns that we were seeing, our goal became the understanding of these patterns, at least in the broadest sense, for possible real-time use (see color plate).

PPIs showing radial velocity components were routinely taken at several selected elevation angles. Since altitude increases with increasing range when the antenna is tilted, each PPI shows a three dimensional picture of environmental wind components combined into one display. In other words, the PPI color display shows a large number of VAD-type (Velocity Azimuth Display) patterns (see: Lhermitte and Atlas, 1961; Browning and Wexler, 1968) simultaneously, where altitude is a function of range.

## 2. PPI APPEARANCE OF HYPOTHETICAL WIND PROFILES

The following is a discussion of Figures 1 through 6, which depict six arbitrary vertical profiles as they would appear on a single Doppler radar PPI display. Each figure shows a combination of hypothetical speed and direction profiles which are, by definition, horizontally homogeneous. Figure 1, for example, represents the appearance of the simplest wind regime, where direction and speed remain constant with height. The contours are velocity components (usually expressed in  $m\ sec^{-1}$ ) with the railroad track representing the 0  $m\ sec^{-1}$  contour. The 0  $m\ sec^{-1}$  contour represents the locus of points where the radar beam is oriented perpendicular to the wind direction, a fact that makes this contour quite handy for determining the azimuthal plane of the wind direction at any point on the contour. If the top of Figure 1 is north, then the radar sees a 0  $m\ sec^{-1}$  component of the wind speed when it is pointed at 30° and 210° azimuth. At these azimuths, then, the radar beam is pointed perpendicular to the wind direction at all ranges (and, therefore, at all heights). The magnitude of the observed wind component increases (as a sine function) as the radar points away from 30° and 210°, until it reaches a maximum value after a 90° change in azimuth, i.e., at 120° and at 300°. At these azimuths, the radar beam is oriented parallel with the wind direction and, therefore, sees a component equal in magnitude to the actual wind speed. Based on these observations, it must be concluded that the wind is coming from either 120° or 300° azimuth, throughout the height range covered by the PPI (The

extent of the height range is, of course, determined by the elevation angle and maximum range of the PPI). We can tell from the Doppler radar data whether the measured velocity component is directed toward or away from the radar. If that information were indicated on Figure 1, then the direction of the wind can be determined. The convention used is for motion away from the radar to be indicated by positive components, and motion toward the radar by negative components. If we arbitrarily decide that in Figure 1, the area to the right of the railroad track (0  $m\ sec^{-1}$  contour) is negative (toward the radar), then we know that the wind is coming from 120° at all altitude levels. If the contour intervals are defined then we know the wind speed.

Figure 2 is similar to Figure 1 in that the 0  $m\ sec^{-1}$  contour is straight. This, again indicates a constant wind direction with increasing height. The other contours, however, are now oriented essentially parallel with the 0  $m\ sec^{-1}$  contour. This configuration results from a wind speed increasing with height. When the radar is looking along a radial perpendicular to the contours, it is looking upwind or downwind. So in this case, as in the first, the wind direction lies along the 120° - 300° plane.

Figure 3 is also a constant direction situation, as seen immediately by the straight 0  $m\ sec^{-1}$  contour. The speed increases with height through half of the altitude interval, and then decreases the exact same amount by the time it reaches the top (or, the farthest range). Each set of closed contours is centered around the point of maximum wind-speed. Again, the wind direction is along the radials which are perpendicular to the contours (120° - 300°, again).

Figures 4 through 6 are analogous to Figures 1 through 3 respectively. The only difference is the change in the behavior of the wind direction. Figures 1 - 3 had a uni-directional wind structure; Figures 4 - 6 have a veering wind with height. The 0  $m\ sec^{-1}$  contour takes on an "S" shape in a veering wind field. The reason for this behavior is straightforward. Remember that the 0  $m\ sec^{-1}$  contour represents the locus of points where the radar beam is perpendicular to the wind direction. Since the direction of the veering wind increases in azimuth with increasing height, the 0  $m\ sec^{-1}$  contour will also increase in azimuth with increasing height and, therefore, with increasing range. This results in the "S" shape seen in the figures. The 0  $m\ sec^{-1}$  contour in a backing wind field will simply have a "backward S" shape (an "2").

The other velocity component contours behave in a way similar to the uni-directional cases, except that they acquire the curvature forced by the changing of the wind direction with height. For example, Figure 4 shows a situation where the wind has a

constant speed at all levels, while the direction is veering. As in Figure 1, the contours all converge into the origin of the display. Figure 5 is similar to Figure 2 in that the wind speed increases with height. The wind direction at any height (a function of range) is  $90^\circ$  from the azimuth of the  $0 \text{ m sec}^{-1}$  contour at that height. The contours, now curved, are no longer parallel to the  $0 \text{ m sec}^{-1}$  contour.

Figure 6 is similar to Figure 3, except for the curvature created by the veering wind direction.

### 3. RAWINSONDE CONVERTED TO RADIAL VELOCITY PPI DISPLAY

In this section we will see that rawinsonde data displayed as a radial velocity PPI will appear as a combination of some of the hypothetical wind fields described in Section 2. A rawinsonde was launched on 16 March 1976 at 2034 EST, during a "Northeast" snow storm. Wind speed and direction were obtained for every 100 meters of the ascent up to the 300 mb level, which was at an altitude of 8836 meters. The task is to transform this information into a PPI display. A  $2^\circ$  elevation angle is used for this example. Table I shows a breakdown of the wind data from the rawinsonde. The first two columns indicate the range from the origin and the height at which a  $2^\circ$  elevation angle will intersect that range. Interpolation of the rawinsonde data provides values of wind speed and direction at these heights.

Table I

Modified Rawinsonde Data, 16 March 1976, 2034 EST

Range (km)	Ht. (m)	Dir. ( $^\circ$ )	Speed ( $\text{m sec}^{-1}$ )
2	70	040	3.2
4	140	044	6.0
6	209	045	8.8
8	279	046	11.6
10	349	049	14.4
12	419	050	16.7
14	489	053	18.5
16	558	054	19.8
18	628	058	21.3
20	698	062	22.3
22	768	065	23.0
24	838	065	23.7
26	907	067	23.1
28	977	072	21.7
30	1047	082	20.3
32	1117	090	18.9
34	1187	100	17.8

Figure 7 shows a radial velocity PPI constructed from the data in Table I. Note, first, that the  $0 \text{ m sec}^{-1}$  contour assumes an "S" shape, but that its curvature varies with range, with the greatest curvature at the larger ranges, and with little or no curvature closer to the origin. This is an indication of the tendency of the wind field to be almost uni-directional at lower levels, before it begins to veer sharply. The pattern within the first 10 km of range has the appearance of the pattern in Figure 2 (constant direction, increasing speed), which reflects the vertical structure depicted by the sounding up to a height of about

350 m. This structure, with only a slight amount of veering extends to about 25 km range on the figure, or up to about 900 m height. Above this, the profile veers at an average rate of  $1^\circ$  for every 8 m altitude, or about  $4^\circ$  for every km range in the figure. The closed contours in the figure give it the appearance of the pattern in Figure 6 (veering wind, increasing then decreasing speed). A check with the data in Table I reveals the fact that this is, indeed, the case. Only two of the six contours on each side of the  $0 \text{ m sec}^{-1}$  contour are closed because the decrease in wind speed is not the same amount as the increase that occurred at lower levels.

Figure A of the color plate is a picture of the color display at  $2.1^\circ$  elevation angle, 2032 EST, two minutes before the rawinsonde was launched. The pattern is almost identical to the rawinsonde PPI pattern, and any dissimilarities are most likely due to the slight difference in effective elevation angle. For example, the veering begins closer to the center of the display in the radar picture because the beam is higher than the trigonometrically derived  $2^\circ$  rawinsonde PPI scan.

The color PPI generally shows a homogeneous wind pattern through the scanned volume. Variations due to convergence, deformation, or particle fallspeed, are not picked up in real time, for they are difficult, or impossible to see on the color display unless they are larger than is usually the case in a stratiform storm.

### 4. TIME AND HEIGHT CHANGES OF RADIAL VELOCITY PPI DISPLAY

Figures A and B on the color plate are pictures of the PPI display taken at 2032 (16 March) and 0104 (17 March), approximately 4.5 hours apart. Both are low elevation angle scans ( $2.1^\circ$ ) showing low-level wind flow. The colors represent wind speed component on a scale from 1 to 99. The portion of the scale above 50 (green to red) indicates motion away from the radar with speed increasing toward higher numbers (reds). The portion below 50 (white, and blue to purple) represents motion toward the radar with speed increasing toward lower numbers (purples). The number 50 corresponds to  $0 \text{ m sec}^{-1}$ . The black band between 47 and 53 on the scale is the  $0 \text{ m sec}^{-1}$  band. The top and bottom ends of the scale are  $22 \text{ m sec}^{-1}$  away from and towards the radar, respectively. For example: 77 means  $27/50 \times 22 \text{ m sec}^{-1}$ , or  $11.9 \text{ m sec}^{-1}$  away from the radar, and 07 means  $43/50 \times 22 \text{ m sec}^{-1}$ , or  $18.9 \text{ m sec}^{-1}$  towards the radar.

In Figure A of the color plate, the flow near the first range ring is from the northeast. There is a wind speed maximum at about  $70^\circ$  azimuth and 20 km range. Some red is seen in the purple region. This is a result of aliasing, which occurs when the speed is greater than the  $\pm 22 \text{ m sec}^{-1}$  unambiguous velocity range of the radar. We call it a "flip-over." From Table I, it can be seen that the maximum low-level wind occurred at around this height and had a value of  $23.7 \text{ m sec}^{-1}$ , which is just over the  $22 \text{ m sec}^{-1}$  limit of the display.

By 0104, Figure B, the storm center had passed to the northeast of the area, and the low level flow had backed to the west of north. The "S" is now on its side, and the speed maxima have shifted about  $70^\circ$  counterclockwise. The maximum speed has



CONSTANT DIRECTION  
CONSTANT SPEED

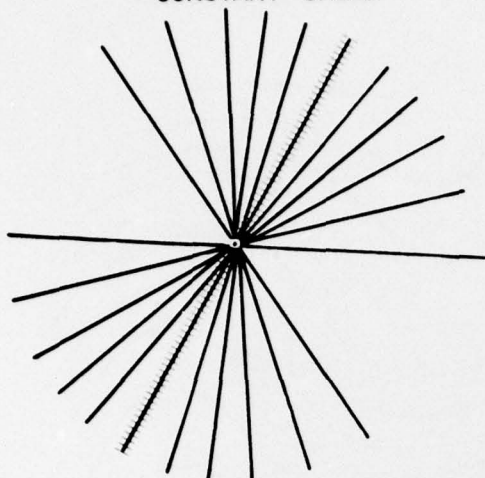


Figure 1.

CONSTANT DIRECTION  
INCREASING SPEED

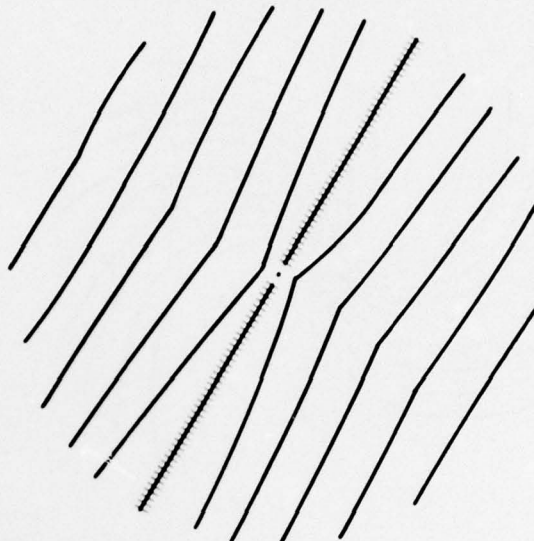


Figure 2.

CONSTANT DIRECTION  
INCREASING, DECREASING SPEED

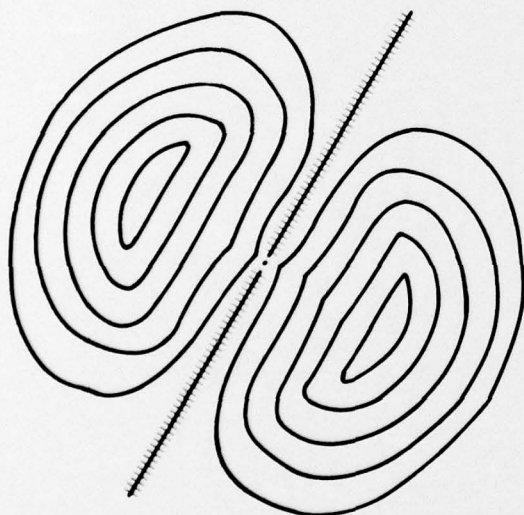


Figure 3.

**COPY AVAILABLE TO DDC DOES NOT  
PERMIT FULLY LEGIBLE PRODUCTION**

Figures 1 - 3. Three arbitrary vertical profiles of hypothetical wind fields as they would appear on a PPI display of mean velocity component. The railroad track represents the  $0 \text{ m sec}^{-1}$  contour. In all three figures, the wind direction is constant with height. Each figure has a brief description of the speed profile it represents. For a complete interpretation of the information contained in these figures, please see the text.

DDC  
RECEIVED  
DEC 29 1978  
REGISTERED

ACCESSION FOR	
NTIS	<input checked="" type="checkbox"/>
U.S.	<input type="checkbox"/>
UNCLASSIFIED	<input type="checkbox"/>
BY	
LIMITATION/AVAILABILITY CODES	
1. A	2. B
3. C	4. D
5. E	6. F
7. G	8. H
9. I	10. J
11. K	12. L
13. M	14. N
15. O	16. P
17. Q	18. R
19. S	20. T
21. U	22. V
23. W	24. X
25. Y	26. Z
27. AA	28. AB
29. AC	30. AD
31. AE	32. AF
33. AG	34. AH
35. AI	36. AJ
37. AK	38. AL
39. AM	40. AN
41. AO	42. AP
43. AQ	44. AR
45. AS	46. AT
47. AU	48. AV
49. AW	50. AX
51. AY	52. AZ
53. BA	54. BB
55. BC	56. BD
57. BE	58. BF
59. BG	60. BH
61. BI	62. BJ
63. BK	64. BL
65. BM	66. BN
67. BO	68. BP
69. BQ	70. BR
71. BS	72. BT
73. BU	74. BV
75. BW	76. BX
77. BY	78. BZ
79. CA	80. CB
81. CC	82. CD
83. CE	84. CF
85. CG	86. CH
87. CI	88. CJ
89. CK	90. CL
91. CM	92. CN
93. CO	94. CP
95. CQ	96. CR
97. CS	98. CT
99. CU	100. CV
101. CW	102. CX
103. CY	104. CZ
105. DA	106. DB
107. DC	108. DD
109. DE	110. DF
111. DG	112. DH
113. DI	114. DJ
115. DK	116. DL
117. DM	118. DN
119. DO	120. DP
121. DQ	122. DR
123. DS	124. DT
125. DU	126. DV
127. DW	128. DX
129. DY	130. DZ
131. EA	132. EB
133. EC	134. ED
135. EE	136. EF
137. EG	138. EH
139. EI	140. EJ
141. EK	142. EL
143. EM	144. EN
145. EO	146. EP
147. EQ	148. ER
149. ES	150. ET
151. EU	152. EV
153. EW	154. EX
155. EY	156. EZ
157. FA	158. FB
159. FC	160. FD
161. FE	162. FF
163. FG	164. FH
165. FI	166. FJ
167. FK	168. FL
169. FO	170. FP
171. FQ	172. FR
173. FS	174. FT
175. FU	176. FV
177. FW	178. FX
179. FY	180. FZ
181. GA	182. GB
183. GC	184. GD
185. GE	186. GF
187. GG	188. GH
189. GI	190. GJ
191. GK	192. GL
193. GO	194. GP
195. GQ	196. GR
197. GS	198. GT
199. GU	200. GV
201. GW	202. GX
203. GY	204. GZ
205. HA	206. HB
207. HC	208. HD
209. HE	210. HF
211. HG	212. HH
213. HI	214. HJ
215. HK	216. HL
217. HO	218. HP
219. HQ	220. HR
221. HS	222. HT
223. HU	224. HV
225. HW	226. HX
227. HY	228. HZ
229. IA	230. IB
231. IC	232. ID
233. IE	234. IF
235. IG	236. IH
237. II	238. IJ
239. IK	240. IL
241. IO	242. IP
243. IQ	244. IR
245. IS	246. IT
247. IU	248. IV
249. IW	250. IX
251. IY	252. IZ
253. JA	254. JB
255. JC	256. JD
257. JE	258. JF
259. JG	260. JH
261. JI	262. JJ
263. JK	264. JL
265. JO	266. JP
267. JQ	268. JR
269. JS	270. JT
271. JU	272. JV
273. JW	274. JX
275. JY	276. JZ
277. KA	278. KB
279. KC	280. KD
281. KE	282. KF
283. KG	284. KH
285. KI	286. KJ
287. KK	288. KL
289. KO	290. KP
291. KQ	292. KR
293. KS	294. KT
295. KU	296. KV
297. KW	298. KX
299. KY	300. KZ
301. LA	302. LB
303. LC	304. LD
305. LE	306. LF
307. LG	308. LH
309. LI	310. LJ
311. LK	312. LL
313. LO	314. LP
315. LQ	316. LR
317. LS	318. LT
319. LU	320. LV
321. LW	322. LX
323. LY	324. LZ
325. MA	326. MB
327. MC	328. MD
329. ME	330. MF
331. MG	332. MH
333. MI	334. MJ
335. MK	336. ML
337. MO	338. MP
339. MQ	340. MR
341. MS	342. MT
343. MU	344. MV
345. MW	346. MX
347. MY	348. MZ
349. NA	350. NB
351. NC	352. ND
353. NE	354. NF
355. NG	356. NH
357. NI	358. NJ
359. NK	360. NL
361. NO	362. NP
363. NQ	364. NR
365. NS	366. NT
367. NU	368. NV
369. NW	370. NX
371. NY	372. NZ
373. OA	374. OB
375. OC	376. OD
377. OE	378. OF
379. OG	380. OH
381. OI	382. OJ
383. OK	384. OL
385. OO	386. OP
387. OQ	388. OR
389. OS	390. OT
391. OU	392. OV
393. OW	394. OX
395. OY	396. OZ
397. PA	398. PB
399. PC	400. PD
401. PE	402. PF
403. PG	404. PH
405. PI	406. PJ
407. PK	408. PL
409. PO	410. PP
411. PQ	412. PR
413. PS	414. PT
415. PU	416. PV
417. PW	418. PX
419. PY	420. PZ
421. QA	422. QB
423. QC	424. QD
425. QE	426. QF
427. QG	428. QH
429. QI	430. QJ
431. QK	432. QL
433. QO	434. QP
435. QQ	436. QR
437. QS	438. QT
439. QU	440. QV
441. QW	442. QX
443. QY	444. QZ
445. RA	446. RB
447. RC	448. RD
449. RE	450. RF
451. RG	452. RH
453. RI	454. RJ
455. RK	456. RL
457. RO	458. RP
459. RQ	460. RR
461. RS	462. RT
463. RU	464. RV
465. RW	466. RX
467. RY	468. RZ
469. SA	470. SB
471. SC	472. SD
473. SE	474. SF
475. SG	476. SH
477. SI	478. SJ
479. SK	480. SL
481. SO	482. SP
483. SQ	484. SR
485. SS	486. ST
487. SU	488. SV
489. SW	490. SX
491. SY	492. SZ
493. TA	494. TB
495. TC	496. TD
497. TE	498. TF
499. TG	500. TH
501. TI	502. TJ
503. TK	504. TL
505. TO	506. TP
507. TQ	508. TR
509. TS	510. TT
511. TU	512. TV
513. TW	514. TX
515. TY	516. TZ
517. UA	518. UB
519. UC	520. UD
521. UE	522. UF
523. UG	524. UH
525. UI	526. UJ
527. UK	528. UL
529. UO	530. UP
531. UQ	532. UR
533. US	534. UT
535. UU	536. UV
537. UW	538. UX
539. UY	540. UZ
541. VA	542. VB
543. VC	544. VD
545. VE	546. VF
547. VG	548. VH
549. VI	550. VJ
551. VK	552. VL
553. VO	554. VP
555. VQ	556. VR
557. VS	558. VT
559. VU	560. VV
561. VW	562. VX
563. VY	564. VZ
565. WA	566. WB
567. WC	568. WD
569. WE	570. WF
571. WG	572. WH
573. WI	574. WJ
575. WK	576. WL
577. WO	578. WP
579. WQ	580. WR
581. WS	582. WT
583. WU	584. WV
585. WW	586. WX
587. WY	588. WZ
589. XA	590. XB
591. XC	592. XD
593. XE	594. XF
595. XG	596. XH
597. XI	598. XJ
599. XK	600. XL
601. XO	602. XP
603. XQ	604. XR
605. XS	606. XT
607. XU	608. XV
609. XW	610. XX
611. XY	612. XZ
613. YA	614. YB
615. YC	616. YD
617. YE	618. YF
619. YG	620. YH
621. YI	622. YJ
623. YK	624. YL
625. YO	626. YP
627. YQ	628. YR
629. YS	630. YT
631. YU	632. YV
633. YW	634. YX
635. YY	636. YZ
637. ZA	638. ZB
639. ZC	640. ZD
641. ZE	642. ZF
643. ZG	644. ZH
645. ZI	646. ZJ
647. ZK	648. ZL
649. ZO	650. ZP
651. ZQ	652. ZR
653. ZS	654. ZT
655. ZU	656. ZV
657. ZW	658. ZX
659. ZY	660. ZZ

VEERING DIRECTION  
CONSTANT SPEED

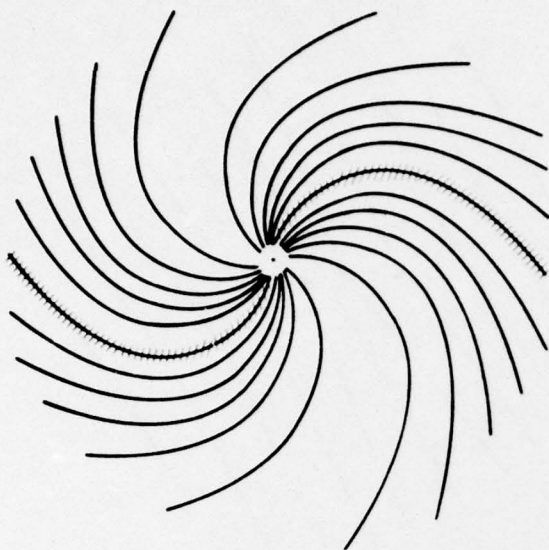


Figure 4.

VEERING DIRECTION  
INCREASING SPEED

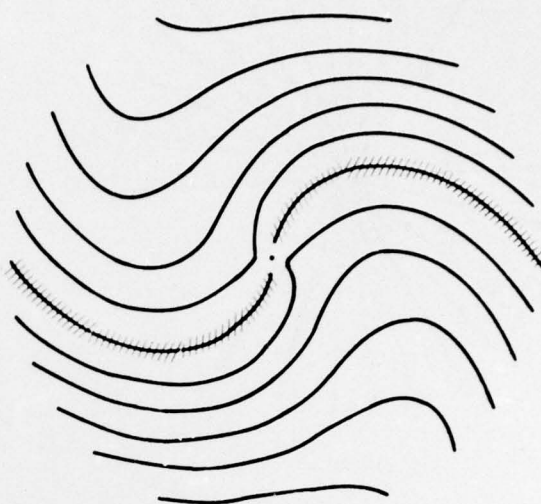


Figure 5.

VEERING DIRECTION  
INCREASING, DECREASING SPEED

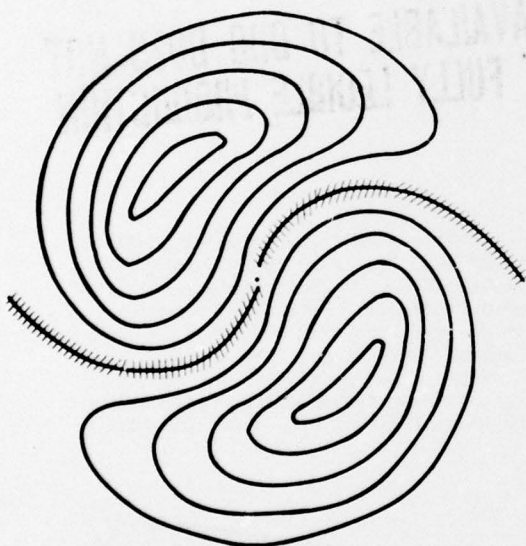


Figure 6.

2° EL 16 MARCH 76  
2034 EST

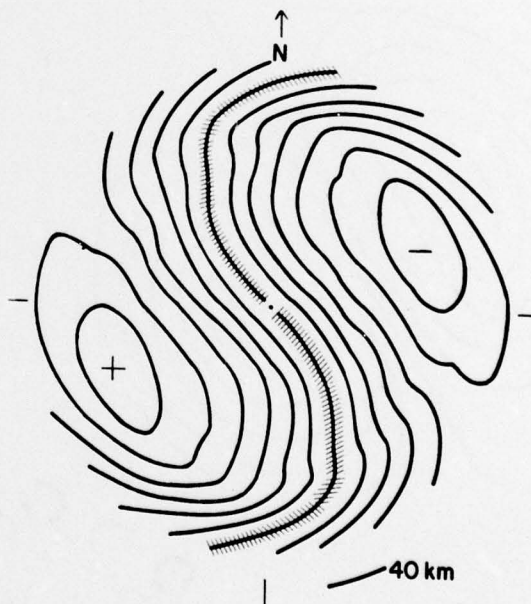


Figure 7.

Figures 4 - 6. These are similar to Figures 1 - 3. In these figures, however, the wind direction veers with height, forcing a change in the appearance of the patterns. The text contains a full explanation of these figures.

Figure 7. Radial velocity PPI constructed from the data in Table I. A  $4 \text{ m sec}^{-1}$  contour is adjacent to the  $0 \text{ m sec}^{-1}$  contour. The interval for the remaining contours is  $3.5 \text{ m sec}^{-1}$ . The minus sign is located at an inbound speed maximum ( $23.7 \text{ m sec}^{-1}$ ). At the plus sign, the maximum is outbound.

decreased to just under 22 m sec<sup>-1</sup>.

Figure C on the plate is a 7.9° elevation angle scan taken earlier during the storm, at 1608 EST. The pattern represents the radar's view of the veering wind field up to about 4400 m altitude. Recall that the plane of the wind is always perpendicular to the azimuth at which the radar beam intersects the 0 m sec<sup>-1</sup> contour (the black band running through the origin). The direction in that plane can be determined by using the color scheme to differentiate motion toward the radar from motion away from the radar according to the procedure explained before. So, we see that at low levels (within about 8 km range) the wind is from the east and southeast with values reaching about 20 m sec<sup>-1</sup> maximum at around 7 km range (or 950 m height). Higher up the wind becomes southwesterly. At these levels the wind speed exceeds the unambiguous velocity range of the display. As before, we experience a "flip-over" from red to purple and vice-versa. For example, looking to the south, we quickly pass through the colors below 50 on the scale and then we see reds, yellow and gray. The gray area represents motion of about 35 m sec<sup>-1</sup> toward the radar, a mid-level speed maximum from the SSW. Above this, the speed decreases again until we run out of echo.

#### 5. SUMMARY AND APPLICATIONS

If a Doppler radar is to be used during the seasons when stratiform-type precipitation is expected, then a guide to the interpretation of data acquired over a large range interval is most useful. Obviously, we do not suggest replacing rawinsondes with Doppler radars, but this quick indication of the flow field is intriguing to work with in real time, as well as beautiful to behold.

A value of contemplating the PPI display of widespread storms is that it gets one geared to observing apparent velocity shear in situations where the displayed shear is a result of either: (1) changes in radar beam viewing angle, or (2) a flow field with vertical veer or shear, or both.

The PPI displays can be readily interpreted by considering the behavior of the 0 m sec<sup>-1</sup> contour to derive information on the wind direction, and the pattern of the other contours to get information on wind speed.

The real-time interpretation of these displays does not enable one to ascertain all of the information that can be obtained from VAD techniques (i.e., convergence, deformation, particle fall speeds). Therefore, it is not possible to draw conclusions on the homogeneity of the observed wind fields unless some radical departures from homogeneity are observed.

Perhaps the final thought that we would like to leave with the reader is the hypothesis that certain characteristics of widespread storms appear in convective storms displayed on the color PPI. In other words, a certain amount of what appears to be "horizontal shear" in convective storms can be explained by considering the Doppler radar viewing angle and the vertical wind shear of the environment. Parts of the convective pattern represent segments, or portions, of the widespread storm picture, with much of the convective activity consisting of echoes with the environmental wind just

flowing through. These would appear as pieces of a stratiform-type velocity display, as though a cookie-cutter had lifted them out (Kraus, 1974). These "flow-through" echoes are not likely to be severe since they have no circulation of their own. A knowledge of the characteristics of the environmental wind field combined with a look at the radial velocity fields in these echoes, might make the problem of severe weather forecasting a bit easier.

#### 6. ACKNOWLEDGEMENTS

The authors are grateful to the members of AFGL's Weather Radar Branch who stayed up all night, through the most recent in a series of St. Patrick's Day snowstorms, in order to collect data. Our thanks also go to the people at the Atmospheric Science Laboratory, Maynard Meteorological Team, who provided the rawinsonde data used in this study, and, as a result, were periodically out in the snow until about 1 AM. June Queijo did an excellent job of manuscript preparation and Pio Petrocchi took the color photographs on the plate.

#### 7. REFERENCES

- Browning, K. A. and R. Wexler, 1968: The determination of kinematic properties of a wind field using Doppler radar. *J. Appl. Meteor.*, **7**, 105-113.
- Jagodnik, A. J., L. R. Novick and K. M. Glover, 1975: A weather radar scan converter/color display. Preprints 16th Radar Meteor. Conf., Boston, Amer. Meteor. Soc., 14-20.
- Kraus, M. J., 1974: Doppler radar investigation of flow patterns within thunderstorms. AFCRL-TR-0290, Environmental Research Papers, No. 481, 86 pp. See Section 6, p.37-45.
- Lhermitte, R. M. and D. Atlas, 1961: Precipitation motion by pulse Doppler. *Proc. Ninth Weather Radar Conf.*, Boston, Amer. Meteor. Soc., 218-223.
- Novick, L. R. and K. M. Glover, 1975: Spectral mean and variance estimation via pulse pair processing. Preprints 16th Radar Meteor. Conf., Boston, Amer. Meteor. Soc., 1-5.



# A NOTE ON THE COLOR DISPLAY

The Porcupine Doppler radar was operating at a pulse repetition frequency of 1613 pps. The maximum range we could see was 1024 cells times 1  $\mu$ s per cell, or 77 km. Our display was operating on a "close-up" mode since we were not seeing precipitation out to the maximum range. An explanation of the housekeeping data follows:

EL 02.1 - 2.1° elevation angle  
 RM = 16 - 16 km range markers  
 TO76: - 76th day of the year, or 16 March  
 20:32 - 8:32 PM, EST

Our maximum unambiguous velocity range while operating at 1613 pps is  $\pm 22$  m sec<sup>-1</sup>, with + indicating motion away from the radar and - indicating motion towards the radar. The threshold values may be defined in terms of speed according to the following table:

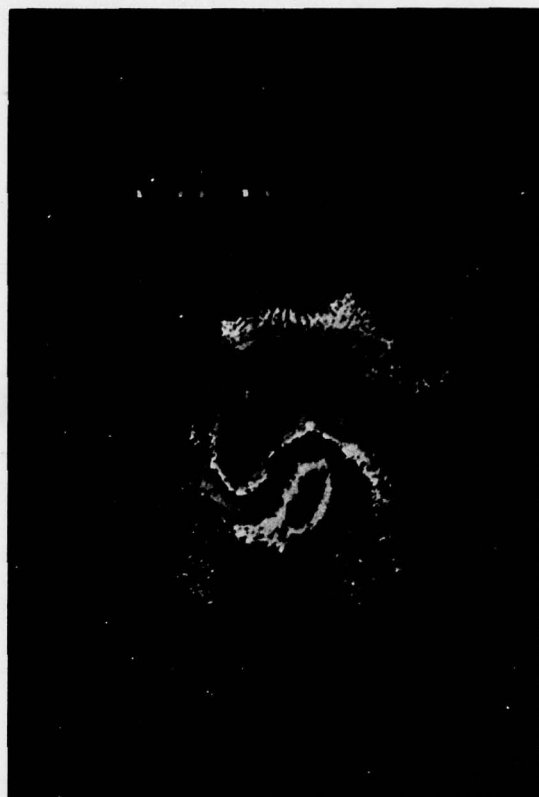
Threshold Value	Velocity (unambiguous) m sec <sup>-1</sup>	Velocity ("flip-over") m sec <sup>-1</sup>
99	+ 21.6	- 22.4
93	+ 18.9	- 25.1
85	+ 15.4	- 28.6
77	+ 11.9	- 32.1
69	+ 8.4	- 35.6
61	+ 4.8	- 39.2
53	+ 1.3	- 42.7
47	- 1.3	+ 42.7
39	- 4.8	+ 39.2
31	- 8.4	+ 35.6
23	- 11.9	+ 32.1
15	- 15.4	+ 28.6
07	- 18.9	+ 25.1
01	- 21.6	+ 22.4

The values in this table are valid only for the unambiguous velocity interval defined by the choice of 1613 pps for our 5.45 cm Porcupine Doppler radar.

We have the freedom to choose four different PRFs: 394, 794, 1613, and 3333. The choice we make depends on the current weather in our vicinity. One must keep in mind that there is the inevitable trade off of range with unambiguous velocity range; if we increase the PRF, we can get a greater unambiguous velocity range at the expense of maximum viewing range. Fortunately, the color display provides us with a certain freedom of choice of range displayed and origin location. This freedom enables us to zero in on points of interest for maximum real-time viewing value.



B



D



A



C



## ANALYSIS OF AN ASYMMETRIC DOPPLER VELOCITY PATTERN

Ralph J. Donaldson, Jr., Rosemary M. Dyer, Michael J. Kraus,  
and James F. Morrissey  
Air Force Geophysics Laboratory  
Hanscom AFB, Massachusetts 01731

### 1. A PUZZLING PATTERN

Following the development and installation of a Pulse Pair Processor (Novick and Glover, 1975) and a color display (Jagodnik et al., 1975) for analysis and presentation of Doppler spectral moments, we have routinely acquired velocity patterns in all available storms, using the 5.5-cm Porcupine Doppler radar. The usual procedure for taking data requires the antenna to scan in azimuth at a constant elevation angle. After each complete rotation, the antenna elevation is stepped up to a new value. The elevation increments are generally  $1^\circ$ , commensurate with the antenna half-power beamwidth of  $0.9^\circ$ , but often larger increments are used above an elevation of  $10^\circ$ . The output of the Pulse Pair Processor, containing information on reflectivity, velocity mean, and velocity variance in each resolution cell, is recorded on tape for subsequent analysis and is presented in real time on the color display in PPI-format. The color display of data taken at any elevation angle above  $0^\circ$  is not, strictly speaking, a plan view of the storm. It is, instead, a conical surface with apex at the radar, slicing across the storm at heights defined by range and elevation angle.

The summer of 1975 in eastern Massachusetts was notable for its scarcity of severe thunderstorms and for occasional intrusions of widespread, winter-type precipitation. A small coastal nor'easter, a weak cousin of the producers of heavy winter-time snow along the Atlantic seaboard, visited our area briefly during the morning of August 7. Precipitation was light, with an average rate of only 0.6 mm/hr, but was sufficient to provide detectable tracers of velocity for our Doppler radar. The storm was scanned in  $1^\circ$ -increments of elevation angle from  $1^\circ$  to  $10^\circ$ .

A photograph of the velocity pattern at elevation  $8^\circ$ , displayed in color, is reproduced as Figure D of the color plate in the preceding paper by Kraus and Donaldson. As in the other figures of this plate, the colors represent contours of velocity, in accordance with the scale on the right of the photograph, ranging from +22 m/s away from the radar (red), down through yellows and greens to black ( $\pm 1.3$  m/s) and on to negative velocities, toward the radar, represented in succession by white, ever-deeper shades of blue, and finally purple indicating velocities up to -22 m/s. The narrow black band separating advancing and receding velocities not only eliminates the stationary ground clutter, but also serves as an indicator of locations where motions within the storm are normal to the radar beam. The two range rings are located at 16 and 32 km.

The puzzling feature of Figure D, and its neighbors at nearby elevation angles, is the asymmetry

of the color patterns. Maximum positive and negative velocities are sensed by the Doppler radar when its antenna beam is pointing downwind and upwind. In a horizontally homogeneous wind field, archetypical of widespread stratiform storms, we would expect Doppler-sensed velocities to decrease uniformly on either side of a maximum, in accordance with the cosine of the directional change of the beam from the velocity maximum. Curiously, though, Figure D shows a concentration of velocity contours near each peak, but each has a long tail trailing clockwise. The pattern resembles the Yin-Yang symbol of Chinese cosmology, or, in a less traditional orientation, two tadpoles chasing one another in a circle.

### 2. SOLUTION OF THE PUZZLE BY FOURIER ANALYSIS

No rawinsonde winds were available on August 7, 1975 for comparison with the Yin-Yang Doppler velocity pattern. Consequently, we generated a wind field from the recorded velocity data, using the precipitation as tracers and following the scheme for Fourier analysis of harmonics developed by Browning and Wexler (1968). Our aim was not only to derive a vertical profile of average wind, but also to gain some knowledge of the uniformity of the wind at each height. At the time of this writing, the harmonic analysis is confined to a quasi-cylindrical section through the storm with a radius of 8.325 km around the radar. This section extends up to a height of 1.45 km, using integral values of elevation angle from  $1^\circ$  to  $10^\circ$ .

Browning and Wexler suggested that the Fourier coefficients of order 0, 1, and 2, which give the horizontal wind field properties of divergence, mean wind velocity, and deformation, respectively, may be computed with sufficient accuracy by summations of Doppler velocities at  $10^\circ$  intervals of azimuth. Accordingly, we sampled the velocities at 36 equally-spaced azimuths around the scanning circle, for each of the eight elevation angles from  $2^\circ$  through  $9^\circ$ . At elevations  $1^\circ$  and  $10^\circ$  we could obtain data at only  $30^\circ$  azimuth intervals, owing to a data gap at elevation  $10^\circ$  and several places at  $1^\circ$  where ground clutter strongly contaminated the precipitation echo. At these two extremes of the elevation angles we computed only the mean wind vector, because we felt that a  $30^\circ$  azimuth spacing was much too coarse for meaningful estimates of divergence and deformation. We will not lay out the computational details here; the reader who may be interested in performing harmonic analyses of Doppler velocities will find all the instructions he needs in the treatise of Browning and Wexler.

Estimates of divergence using Doppler velocities acquired at elevation angles above  $0^\circ$  are contaminated by a small component of precipitation fall speed moving toward the radar. We did not measure the vertical speed of the raindrops, but on the basis of

## DOCUMENT CONTROL DATA - R&amp;D

Security classification of title, body of abstract and indexing annotation must be entered when the overall report is classified

1. ORIGINATING ACTIVITY (Corporate author)		2a. REPORT SECURITY CLASSIFICATION	
Air Force Geophysics Laboratory (LYW) Hanscom AFB Massachusetts 01731		Unclassified	
3. REPORT TITLE		2b. GROUP	
INTERPRETATION OF PPI VELOCITY DISPLAYS IN WIDESPREAD STORMS			
4. DESCRIPTIVE NOTES (Type of report and inclusive dates)			
Scientific. (9) Interim. rept.			
5. AUTHOR(S) (First name, middle initial, last name)			
Michael J. Kraus Ralph J. Donaldson, Jr. (11) 7 Dec 76 (12) 8p.			
6. REPORT DATE		7a. TOTAL NO. OF PAGES	7b. NO. OF REFS
7 December 1976		5	5
8a. CONTRACT OR GRANT NO.		9a. ORIGINATOR'S REPORT NUMBER(S)	
(16) 66720301		(14) AFGL-TR-76-0283	
b. PROJECT, TASK, WORK UNIT NOS.		9b. OTHER REPORT NO(S) (Any other numbers that may be assigned this report)	
c. DOD ELEMENT (12) 43 62101F			
d. DOD SUBELEMENT			
10. DISTRIBUTION STATEMENT			
Approved for public release; distribution unlimited.			
11. SUPPLEMENTARY NOTES		12. SPONSORING MILITARY ACTIVITY	
Reprinted from Preprint Volume, 17th Conference on Radar Meteorology, Oct 26-29, 1976, Seattle, Washington		Air Force Geophysics Laboratory (LYW) Hanscom AFB Massachusetts 01731	
13. ABSTRACT			
<p>→ AFGL's Porcupine Doppler radar observed several New England winter storms, both snow and rain. A pulse-pair processor, linked to a color display, provided contours of the mean velocity structure within these storms. The data were recorded on digital tape, and subsequently played back on the color display for further viewing and analysis. Six hypothetical wind fields were transformed into PPI pictures analogous to those produced by the Doppler radar. They provided a basis for interpreting the measured wind fields. Rawinsondes launched close to the radar site provided data which, when similarly transformed were readily comparable to the radial velocity fields generated by the radar. The characteristics of these velocity fields are discussed. Reference is made to individual synoptic situations, their change with time, and the Doppler radar's portrayal of these events. ↖</p>			
KEYWORDS: Doppler radar, Radial velocity pattern, Pulse pair processor, Color display, Wind field			